lubricants

MDPI

Piston-Pin Rotation and Lubrication

Hannes Allmaier * and **David E. Sander**

VIRTUAL VEHICLE Research GmbH, Inffeldgasse 21A, 8010 Graz, Austria; david.sander@v2c2.at
* Correspondence: hannes.allmaier@v2c2.at

check for
updates

Abstract: The rotational dynamics and lubrication of the piston pin of a Gasoline engine are investigated in this work. The clearance plays an essential role for the lubrication and dynamics of the piston pin. To obtain a realistic clearance, as a first step, a thermoelastic simulation is conducted for the aluminum piston for the full-load firing operation by considering the heat flow from combustion into the piston top and suitable thermal boundary conditions for the piston rings, piston skirt, and piston void. The result from this thermoelastic simulation is a noncircular and strongly enlarged clearance. In the second step, the calculated temperature field of the piston and the piston-pin clearance are used in the simulation of the piston-pin journal bearings. For this journal bearing simulation, a highly advanced and extensively validated method is used that also realistically describes mixed lubrication. By using this approach, the piston-pin rotation and lubrication are investigated for several different operating conditions from part load to full load for different engine speeds. It is found that the piston pin rotates mostly at very slow rotational speeds and even changes its rotational direction between different operating conditions. Several influencing effects on this dynamic behaviour (e.g., clearance and pin surface roughness) are investigated to see how the lubrication of this crucial part can be improved.

Keywords: combustion engine; friction; journal bearing simulation; piston pin

1. Introduction

From all journal bearings that are employed in an internal combustion engine, the piston pin has to endure the most extreme working conditions, as it suffers from insufficient, random lubrication, and has to withstand extreme forces. An exemplary piston pin from a fired engine showing typical wear marks is shown in Figure 1. It is a critical part, as failure of the piston pin generally results in fatal damage for the combustion engine. In the development of new, highly efficient engine generations with high power to volume displacement ratios, the occurrence of failures of the piston pin increases. In these cases, there generally exists little understanding as to what the causes of these failures are and how they can be prevented; consequently, a costly trial-and-error approach is taken to fix these issues. This work aims to provide a fundamental basis for the understanding of the lubrication of the piston pin as well as to investigate how standard optimization measures (like changing clearance or reducing surface roughness) affect it.

There exist only few works in literature that investigate the lubrication of the piston pin. The reason for this situation lies in the complexity that is required to investigate the lubrication of the involved piston-pin journal bearings.

Technically, the piston pin of internal combustion engines connects three journal bearings that are being formed by the pin with the two piston bosses and the small end section of the con-rod. However, in contrast to the other well-known highly stressed journal bearings in an internal combustion engine,

the piston pin (as it is used today) is freely floating and does not move following a determined motion. The rotation of the piston pin is the result of the friction between the piston pin, the two piston bosses, and the small end of the con-rod. Any small change in friction whatsoever will affect the rotation of the piston pin, which again will affect its friction. This is a highly challenging problem for simulation and a number of works numerically investigate the piston pin [3–5].
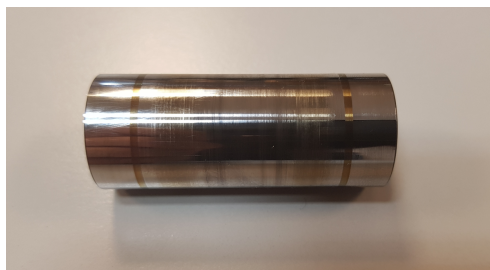

Figure 1. Piston pin after a fired engine test showing typical wear marks from edge contact with the con-rod and the piston bosses.

Experimentally, the extremely small space surrounding the piston pin makes it difficult to install sensors to detect the movement of the piston pin. In addition, telemetry is required to transfer signals from the moving parts and also the high temperatures around the piston pin of about 160 °C exceed typically the maximum temperature permissible for electronic parts. For these reasons, there exist only few works in literature that investigate the movement and lubrication of the piston pin experimentally [6–8].

Numerically, the freely floating piston pin represents an ill-conditioned system, as the calculation of the lubricating film and the movement of the piston pin are strongly coupled. Convergence problems are the typical result. Further, the three journal bearings formed together with the piston pin suffer from insufficient lubrication, as in most engines there exists no explicit oil supply for these bearings—these three journal bearings are only lubricated by the oil mist generated by the main and big end bearings and/or piston oil jets. Due to the very high loads acting on the piston pin, in combination with its very slow rotation [4,5] extremely high temperatures [9–12], mixed lubrication is dominant for these three journal bearings [5]. Consequently, conventional purely hydrodynamic lubrication theory cannot be applied and an asperity friction model which realistically describes mixed lubrication is required.

2. Introduction to Journal Bearing Lubrication

A reliable lubrication system is of key importance for internal combustion engines. For emission legislation, the focus lies on the mechanical friction losses of the engine as these directly contribute to fuel consumption. Consequently, OEMs continually work to reduce these to a minimum. However, there exist different forms of friction that are usually represented as the Stribeck curve: purely hydrodynamic lubrication, boundary friction, and the mixed lubrication regime, where both of these different forms of friction coexist. These different regimes are shown for a statically loaded journal bearing in Figure 2.

Now, lubricated contacts—as they are present in internal combustion engines—might be assumed to operate in purely hydrodynamic lubrication. For this form of lubrication, a sufficiently thick oil film separates the two gliding surfaces from each other and the friction in this oil film generates the observed losses. Purely hydrodynamic lubrication is advantageous in principle as there is no actual contact between the surfaces—and consequently, no wear can occur. Of course, the reality is more complex as already the transient nature of operation for internal combustion engines prevents pure hydrodynamic lubrication (e.g., during starting).

Further, the Stribeck-curve shows that the minimum of the friction losses is located in the mixed lubrication regime where some surface contact is present. Consequently, the continued efforts to reduce the friction losses in internal combustion engines have led to the regular appearance of mixed lubrication. Excessive wear is typically countered with either oil-additive chemistry or surface coatings and is often combined with a very smooth surface topography.
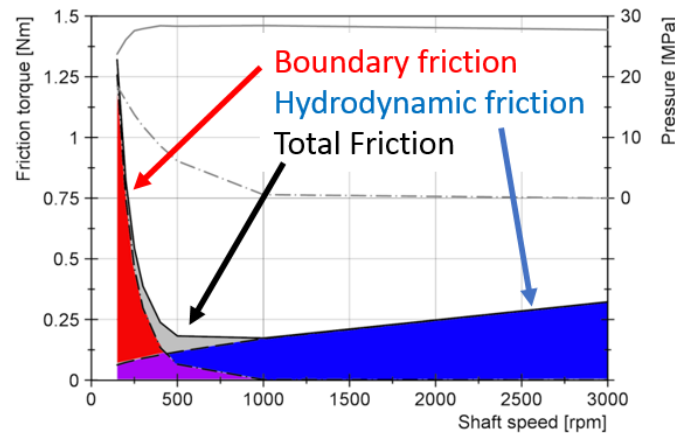

Figure 2. Stribeck-curve for a statically loaded journal bearing (from [13]). As can be seen, with decreasing shaft speed, mixed lubrication starts early at about ca. 1000 rpm and steadily increases. The total friction reaches its minimum at about 500 rpm, where significant mixed lubrication is present and accounts for about one third of the total friction.

2.1. Engine and Oil to Be Investigated

The engine to be investigated is a turbocharged, 4-cylinder inline gasoline engine with 1.8 l volume displacement and a nominal power of 130 kW; its technical data are summarized in Table 1. This engine was already part of previous works of the authors on engine friction [14,15], where it was termed *Gasoline 1* engine.

Within this work, the same engine oil of previous works of the authors [14,15] is also investigated; the basic lubricant data is listed in Table 2.

2.2. Simulation Methodology

Accurately simulating the large range of operating conditions of journal bearings that extend from fully hydrodynamic lubrication to severe mixed lubrication involves many factors. As it is not possible to discuss these in deserved detail here, the authors refer to the original works [16,17], where the specific points are not only discussed in depth, but which also contain the relevant references to previous works. In the following, only a brief discussion of the key points and related references is given for this reason.

The basic simulation consists of a multibody system with elastically deformable finite element bodies, which are represented as condensed structures with reduced degrees of freedom [18,19]. The bodies are coupled with an oil film that is described using the Reynolds equation, with extensions developed by Patir and Cheng [20,21], to consider the effects of surface roughness on very small oil-film thicknesses:

$$-\frac{\partial}{\partial x}\left(\phi_x\theta\frac{h^3\rho}{12\overline{\eta}}\frac{\partial p}{\partial x}\right) - \frac{\partial}{\partial y}\left(\phi_y\theta\frac{h^3\rho}{12\overline{\eta}}\frac{\partial p}{\partial y}\right) + \frac{\partial}{\partial x}\left(\theta h\rho\frac{u_1+u_2}{2}\right) + \frac{\partial}{\partial x}\left(\phi_s\theta\rho\frac{u_1+u_2}{2}\sigma_s\right) + \frac{\partial}{\partial t}(\theta h\rho) = 0, \qquad (1)$$

where x is the circumferential and y the axial direction. p and h represent the local hydrodynamic pressure and oil-film thickness. u_1 and u_2 denote the sliding speeds of the facing surfaces. The pressure flow factors ϕ_x, ϕ_y and the shear flow factor ϕ_s consider rough surfaces. The oil viscosity $\bar{\eta}$ is also a function of x and y and depends on local temperature, pressure, and shear rate. To consider cavitation in the low-pressure region, the mass-conserving cavitation model based on the Jakobsson–Floberg–Olsson (JFO) approach is used [22]. Θ represents the fill ratio for the mass-conserving cavitation model. In the cavitation region, the hydrodynamic pressure p becomes the cavitation pressure and the fill ratio is below 1. In the lubricated region (high-pressure region), where p is above cavitation pressure, the fill ratio becomes 1.

Table 1. Technical data of the investigated engine.

Parameter	Gasoline-Engine 1
Volume displacement	1781 cm^3
Compression ratio	9.5:1
Bore	81 mm
Stroke	86.4 mm
Nominal torque	235 Nm
Nominal Power	130 kW
Specific power	72 kW/L
Maximum Speed	6600 rpm
Piston pin outer diameter	20 mm
Piston pin inner diameter	12 mm
Piston pin nominal radial clearance	6 µm
Piston pin length	68 mm
Piston boss length	20 mm
Small end length	25 mm
Con-rod length	144 mm
Main bearing diameter	54 mm
Main bearing width	22 mm
Main bearing clearance (cold)	20 µm
Big-End bearing diameter	47.8 mm
Big-End bearing width	25 mm

Table 2. Basic rheological properties of the lubricant.

SAE class	5W30
Density at 15 °C	853 kg/m^3
Dynamic viscosity at 40 °C	59.88 mPas
Dynamic viscosity at 100 °C	9.98 mPas
HTHS viscosity	3.57 mPas

(HTHS: high-temperature high-shear-rate viscosity (defined as the dynamic viscosity of the lubricant measured at 150 °C and at a shear rate of 10^6 s^{-1}).

The complex lubricant rheology requires the consideration of the piezoviscous effect (increase of viscosity with increase of pressure), as well as taking into account the non-Newtonian behaviour (viscosity reduction due to high shear rates) of multigrade hydrocarbon-based lubricants. The method used in this work utilizes measured rheological data for these two effects and includes a correction to yield the correct high-temperature high-shear-rate viscosity (HTHS)-viscosity (The HTHS-viscosity is defined as the viscosity at high temperature (150 °C) and high shear rate (10^6 1/s).) (see in particular, [23,24]). The lubricant rheology used in this work is also presented in detail in the next Section 2.2.1.

To describe the occurrence of metal–metal contact in the simulation of an asperity contact model, a suitable boundary friction coefficient that considers the presence of friction-modifying additives [25]

and the surface roughnesses of the involved surfaces are required. The method used in this work employs the very well-known Greenwood–Tripp model [26] in combination with surface roughness data from measured surfaces (for details, see in particular, [23,24,27]). Accordingly, the asperity contact pressure p_a is calculated as follows:

$$p_a = KE^* F_{\frac{5}{2}}(H_s),\tag{2}$$

where H_s is a dimensionless clearance parameter, E^* is the composite elastic modulus, and K is the elastic factor which depends on surface roughness, asperity radius, and asperity density. $F_{\frac{5}{2}}$ is a form factor defined by Greenwood and Tripp [26]. The shear stress due to asperity contact is calculated by multiplying the asperity contact pressure with a boundary friction coefficient μ_{Bound}:

$$\tau_a = \mu_{Bound} \cdot p_a,\tag{3}$$

where it was found in previous works [23,24] that a μ_{Bound} of 0.02 gives a close agreement with experimental data.

In addition, it is crucial to use realistic surface shapes for the bearing edges (microgeometry) in the simulation as otherwise the metal–metal contact is largely overestimated [24,27]. Finally, the thermal processes within the oil film as well as the heat transfer to its surroundings need to be considered suitably. In [28], the thermal processes of journal bearings under high dynamic loads are investigated in direct comparison to experimental data. It was shown that it is possible to reproduce the thermal properties of the journal bearings very accurately in comparison to experimental measurements. It was found that the stable thermal behaviour of the lubricant film in journal bearings can be very well described by an isothermal elastohydrodynamic (EHD) simulation method [19] in combination with a suitable equivalent temperature that describes the temperature gradient in the journal bearing. From these results [28], a very simple equivalent-bearing temperature relation was derived for the isothermal EHD-simulation that is consequently able to predict the journal bearing friction losses very accurately for a large range of different lubricants, journal speeds, and loads, as was shown in direct comparison to experimental data (see in particular, [23,24]). A complete and exhaustive discussion of these points is given in two open-access published book chapters [16,17] (the cited book chapters can be downloaded for free at [1]).

Due to the inherent convergence issues with the piston-pin simulation, at least 9 working cycles (6480° crank angle) were simulated in total for every investigated case. Typically it was found—and an example is shown in Figure 3—that the simulation needs 2–3 working cycles to reach a state which no longer changes completely in comparison to later cycles. While there exist smaller differences between later cycles and no ideal periodicity is achieved, the last 3 working cycles were averaged to ensure that the results are reliable. Especially, the investigated operating conditions involving part-load operation caused very slow resulting piston-pin rotations close to 0 rpm, which posed the biggest challenges numerically with the largest variations between cycles. Consequently, 18 working cycles have generally been simulated for part-load operation points to have enough data for a meaningful analysis of these operating points.

In the simulation, the reference case was defined with a surface roughness of 0.06 μm for the piston pin [8] and 0.15 μm for the small end and piston boss, respectively; in addition, the piston-pin clearance was defined with 6 μm.

In addition, several variants have been investigated: different piston-pin clearances (4 and 9 μm) as well as a reduced surface roughness (0.02 μm), which are in agreement with the range of values found in literature [8,29,30]. All variants are summarized in Table 3.
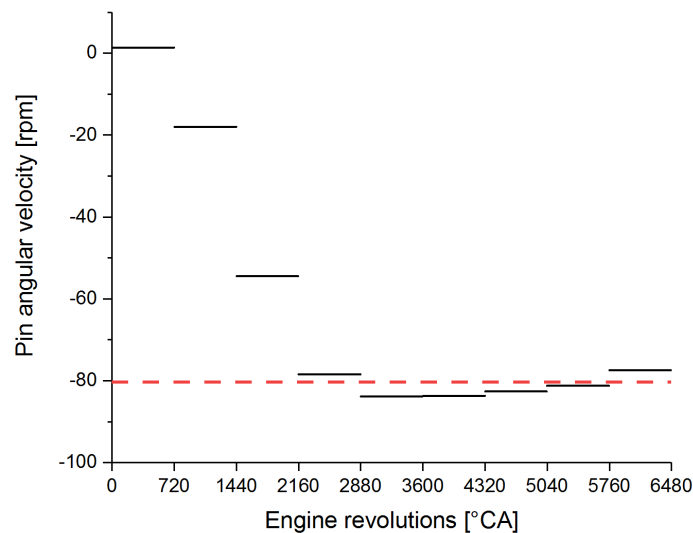
Figure 3. An exemplary result of the convergence behaviour of the presented piston-pin simulation: shown is the 720° averaged angular velocity of the piston pin for all 9 engine working cycles for 3000-rpm engine speed and full-load operation. Typically, the first 2–3 engine working cycles are needed for the simulation to reach a state which no longer changes completely in comparison to later cycles. The last 3 working cycles are evaluated for the results (shown as red dashed line for comparison).

Table 3. Investigated surface and clearance variants

	Reference	Variant 1	Variant 2	Variant 3
Surface roughness piston pin	0.06 μm	0.06 μm	0.06 μm	0.02 μm
(Cold) Clearance piston pin	6 μm	4 μm	9 μm	6 μm

2.2.1. Oil Rheology in the Simulation

To describe the physical properties of the lubricant realistically, an extensive rheological model is employed for the description of the 5W30 lubricant (as described by Table 2) in the simulation [16,17].

Both the effects of pressure p (piezoviscous effect) as well as the influence of local shear rate $\dot{\gamma}$ (non-Newtonian effect) are considered in the simulation of the lubricant film by employing the well-known Barus and Cross equations; the viscosity (η) over temperature (T) relation is described using the Vogel equation [16,17]:

$$\eta(T, p, \dot{\gamma}) = A \cdot e^{\frac{B}{T+C}} \cdot e^{\alpha \cdot p} \cdot \left(r + \frac{1 - r}{1 + (K \cdot \dot{\gamma})^m} \right). \tag{4}$$

The applied parameters are listed in Table 4 and are calculated using results from previously published work [23] and from lubricant characteristics obtained from laboratory oil analysis.

Table 4. Rheological parameters for Equation (4) of the Fuchs 5W30 lubricant.

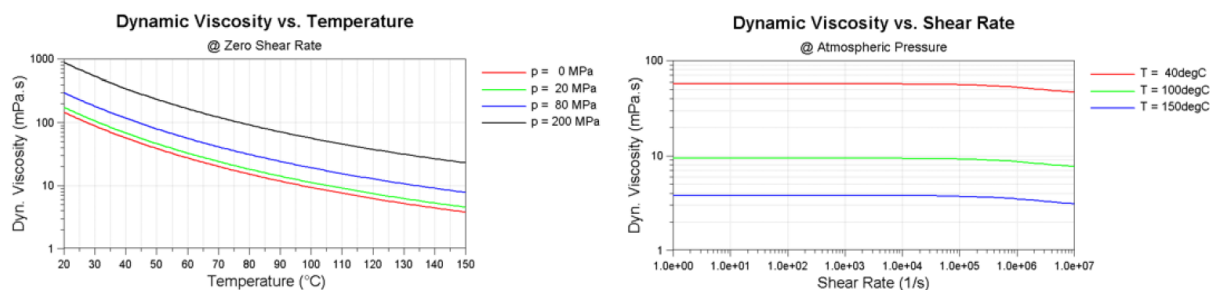|		
A	0.064	mPa s
B	1124.7	°C
C	125.48	°C
m	0.79	-
α	0.0009	1/bar
r	0.75	-
K	3.5 e-7	s

For the description of the pressure- and temperature-dependent density, the widely used Dowson/Higginson equation is used (see Equation (5)), applying the parameters listed in Table 5.

$$\rho(p,T) = \rho_0 \cdot \left(1 + \frac{f_1 \cdot p}{1 + f_2 \cdot p}\right) \cdot (1 - f_3 \cdot (T - T_0)).\tag{5}$$

Table 5. Rheological parameters for Equation (5) of the SAE 5W30 lubricant.

ρ_0	853	kgm^3
T_0	15	°C
f_1	0.001	1/MPa
f_2	0.003	1/MPa
f_3	$8.5e^{-}4$	1/°C

Figure 4 shows the resulting dynamic viscosity of the lubricant.

Figure 4. Dynamic viscosity of the investigated 5W30 engine oil for different temperatures, pressures, and shear rates, as used in the simulation (from [31]).

2.3. Thermoelastic Simulation of the Piston

In internal combustion engines, pistons made from aluminum are commonly used in combination with piston pins made from steel. These two different materials not only have a very different thermal expansion behaviour, but there also exists a very strong local temperature gradient between the piston top and the piston skirt. Both of these factors have a strong impact on the actual piston-pin clearance which does not only change strongly in magnitude but also becomes noncircular. This change in clearance can not only affect piston-pin friction [32] and wear, but might also lead to a strongly increased noise emission [33,34].

The thermal simulation has been conducted using Simulia's [2] *Abaqus* finite element solver package using a two step process:

The first step is to solve the heat-diffusion equation to obtain the temperature field for the piston. To realize this, suitable thermal boundary conditions have to be defined. As thermal diffusion processes are slow compared to the mechanical oscillation of the components [35], a static heat analysis was performed. A heat power of 4.5 kW (corresponds to a heat flow of 9×10^5 W/m^2) originating from combustion during full-load operation of the engine was defined to enter the piston top homogeneously. Further, so-called surface film temperatures and film coefficients were defined for different specific parts of the piston, which represent thermal boundary conditions describing the heat flow into the cylinder liner and to the oil mist inside the crank case. Surface-film temperature for the top ring, 2nd and oil ring, and piston skirt were defined as 160 °C, 130 °C, and 100 °C, respectively. Inside the piston void, the piston is able to conduct heat to the crank case oil mist by defining the corresponding surface film as having a temperature of 80 °C. These thermal boundary conditions are shown graphically in Figure 5.

While the exact heat flows of this particular engine are not known and suitable assumptions had to be taken, it is of more importance for this work to ensure that a realistic temperature field for the piston is obtained from the performed thermoelastic simulation. In comparison to more detailed thermal simulations [36], and in comparison to the temperature measurements available in literature [8–12], the obtained piston temperatures are in good agreement and are shown in Figure 6.

The second step of the thermal simulation is to use the obtained temperature field from the first step to calculate the resulting thermoelastic deformations of the piston. The resulting deformations are several orders of magnitude smaller than the geometrical dimensions of the piston, which justifies to treat these two simulation steps independently of each other. The obtained thermoelastic deformations are shown magnified by a factor of 100 in Figure 7.

Defined surface film temperatures on:

Top ring: 160°C
2nd and oil ring: 130°C

Piston skirt: 100°C

Piston void: 80°C

Figure 5. The figure shows the actual piston investigated in this work together with the thermal boundary conditions used in the thermal simulation. Surface-film temperatures have been defined for the top ring, the 2nd and oil ring, the piston skirt, and for the inner-piston void volume.
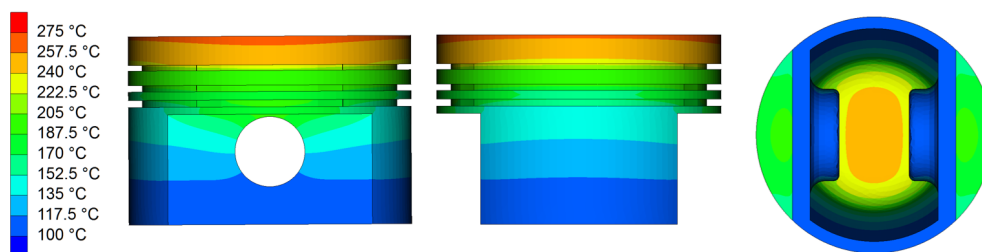
Figure 6. The figure shows the piston temperature field obtained from the thermoelastic simulation with temperatures ranging from 275 °C on the piston top to 105 °C on the piston skirt.
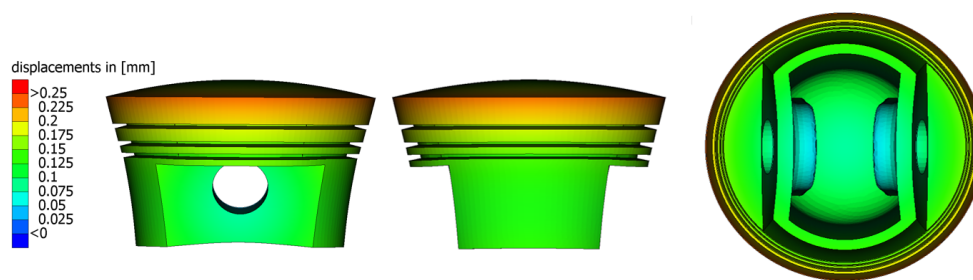

Figure 7. Thermoelastic deformations obtained from the simulation shown schematically; the resulting deformation is shown magnified by a factor of 100 to make the deformations visible.

The central result of this thermal analysis are the thermoelastic deformations that yield a noncircular and much enlarged clearance between the piston pin and the piston bosses, see Figure 8, where the thermal expansion of the piston pin has already been considered (With a piston-pin temperature of 160 °C, the pins expand radially by about 9 μm.).
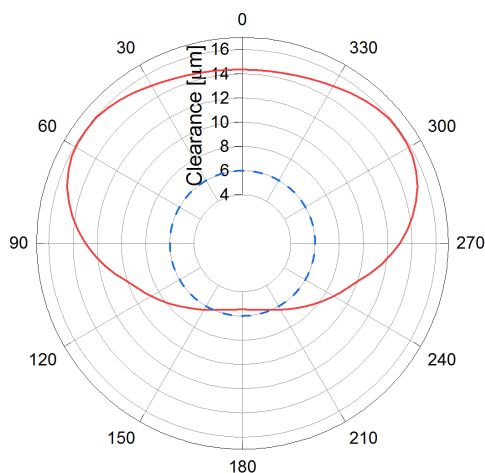

Figure 8. Noncircular and strongly enlarged radial clearance ranging from 10–15 μm between piston pin and piston boss, resulting from the thermoelastic deformation of the aluminum piston and steel piston pin (shown as solid red line). In comparison, the nominal cold radial clearance of the piston pin is defined with 6 μm (shown as dashed blue line for comparison).

For the piston pin to the con-rod small-end journal bearing, the clearance is not so strongly affected by the thermoelastic deformations as both parts (pin and con-rod) are made from steel. Therefore, a piston pin to small-end clearance of 6 μm is used for the following investigations.

2.4. Simulation of the Piston Pin

For the simulation of the three oil films that support the piston pin, the following oil-film temperatures have been defined:

Piston boss: Due to the strong local temperature gradients, a pure isothermal oil-film simulation would be a strong simplification of the real situation. On the other hand, performing a full thermoelastohydrodynamic (TEHD) simulation considering the energy and heat equation—as was done by the authors in a previous work for a heavy loaded main bearing [28]—is also not feasible. The simulation of a freely floating pin is already numerically intensive and plagued with poor convergence. Therefore, it is uncertain whether a combination with a full TEHD would—even with a huge numerical effort—lead at all to converged results. However, in contrast to the heavy loaded main and big end bearings where the actual friction in the oil film causes the temperature field, the situation is very different for the piston pin. For the piston pin, it is not the friction power loss in the oil film that generates the temperature field, but it is caused by the heat flow from the combustion (see also [8]). Therefore, a suitable approach is to directly consider the temperature field from the piston thermal analysis in the EHD-simulation.

For the piston bosses, the locally varying temperature field from the thermal analysis is used in the EHD-simulation, see Figure 9.

For the parts of the piston pin that are supported by the piston bosses, a temperature of 160 °C is used in the simulation. This temperature represents roughly the average of the circumferentially varying piston boss temperature field [8], which is justified due to the rotation of the pin. For the actual oil-film simulation, the average of both (local) temperatures is used for every circumferential point.
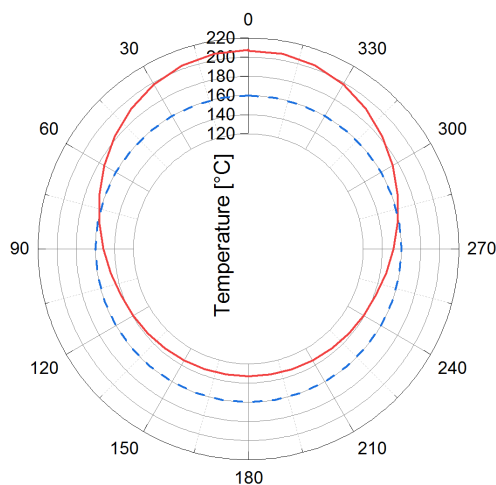

Figure 9. Temperatures used for the oil-film simulation of the piston boss journal bearing obtained from the thermal analysis (plotted as solid red line, see text). For comparison, the piston-pin temperature defined for the oil-film simulation is also shown (blue dashed line).

Small end: For the simulation of the small end journal bearing—which is not in direct contact to the piston—a constant 130°C oil-film temperature is defined.

3. Causes of Changing Piston-Pin Dynamics

The friction moment originating in the two piston bosses and the small end journal bearings causes the rotation of the piston pin. The friction moment caused by the two piston boss journal bearings counteracts the friction moment caused by the small end journal bearing, so the resulting net friction moment actually rotating the piston pin is considerably smaller then these moments. This is shown for the 1000 rpm part-load case in Figure 10.
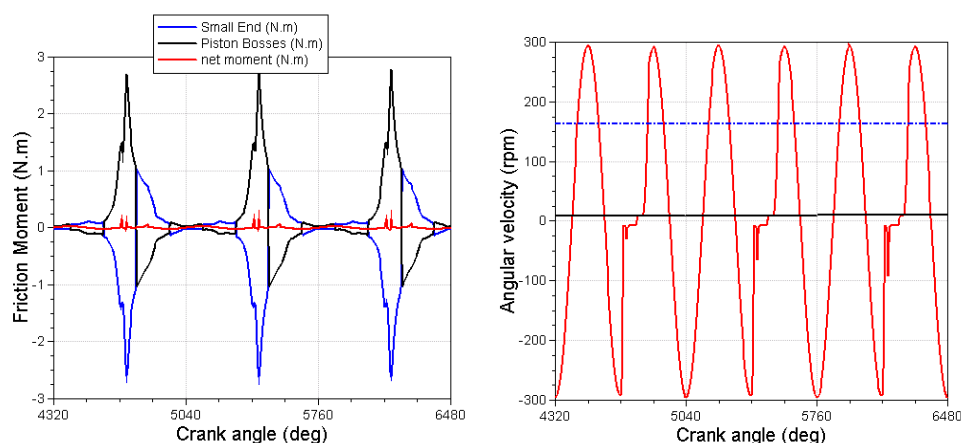

Figure 10. Left: Friction moment originating from the small end (blue line) and the two piston boss journal bearings (black line); these friction moments counteract each other and result in a significantly smaller net friction moment (shown in red) which actually causes the piston-pin rotation. **Right**: Resulting angular velocity of the piston pin (red) and 720° averaged resulting velocity (black); for comparison, the average absolute angular velocity is also shown as a blue dashed line.

As this resulting net friction moment is very small, it reacts very sensitively to any change in external factors like engine load, speed, clearance, etc. Although the friction moments shown in Figure 10 appear to be rather large, with maximums of up to almost ± 3 Nm, the resulting net moment reaches a maximum of less than 0.2 Nm and causes an average piston-pin rotation of only 8 rpm (see also Figure 10). Higher engine speeds cause even smaller friction moments for the small end and piston boss journal bearings. As also can be seen from Figure 10, the resulting net friction moment is of first order in relation to engine speed and causes a strongly oscillating movement of the piston pin with the crank shaft frequency. Concerning the actual piston-pin lubrication, not only the average piston-pin angular velocity is important, but also the average absolute angular velocity due to the strong oscillating movement. The average absolute angular velocity is calculated as the average of the absolute value of the angular velocity and can only indicate average rotation speed, but not direction. So, for the shown 1000 rpm engine speed and part-load case, the results show that the piston pin oscillates strongly with an average absolute angular velocity of about 160 rpm, but shows globally an almost zero average piston-pin angular velocity.

4. Piston-Pin Dynamics and Lubrication for Different Engine Operating Conditions

As outlined in the introduction, little experimental information is available in literature on the movement of the piston and how different engine operating conditions affect it and its lubrication. Consequently, in the following, different engine operating conditions are investigated, see Table 6.

Table 6. Engine operating conditions investigated (WOT refers to wide open throttle), which means full load.

Engine Speed	Engine Load	Peak Cylinder Pressure
1000 rpm	half load	40 bar
1000 rpm	WOT/full load	80 bar
3000 rpm	half load	40 bar
3000 rpm	WOT/full load	80 bar
6000 rpm	half load	40 bar
6000 rpm	WOT/full load	80 bar

The obtained results are very interesting, as the average rotational speed of the piston pin varies greatly and even changes its direction of rotation depending on engine operating point, see Figure 11. It appears that engine load generally leads to faster pin rotation while part-load operating conditions cause very slow, close to stand-still rotation of the piston pin. Further, it is interesting to note that for one engine speed (3000 rpm), a negative piston-pin rotation is obtained (The positive direction of rotation is defined as being equal to the direction of the crank shaft rotation) which changes into positive direction for high engine speeds (e.g., 6000 rpm). Consequently, between 3000 and 6000 rpm there exists an engine speed for which full-load operation also causes an almost zero rotation speed of the piston pin.
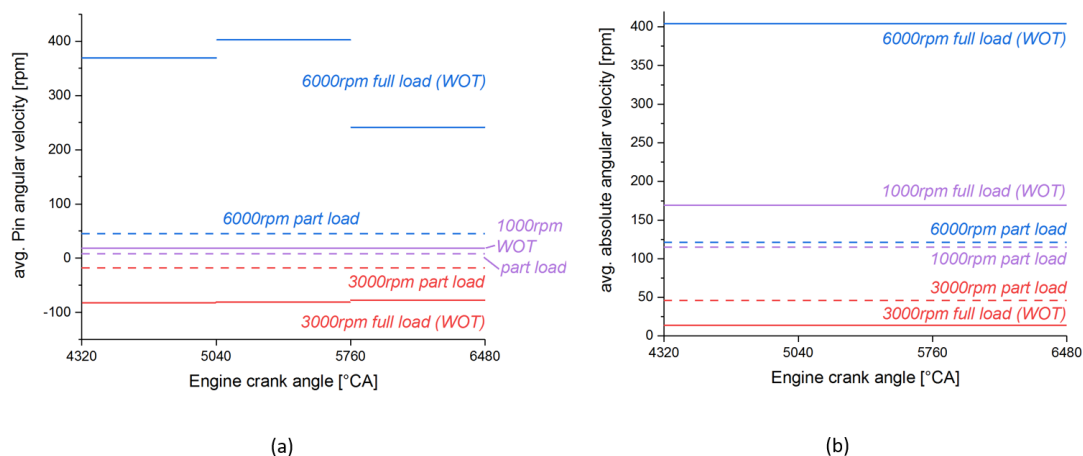
(a)

(b)

Figure 11. (**a**) The average rotational speed of the piston pin shown for different operating conditions: as can be seen, part-load operating conditions (shown as dashed lines) lead to very low angular velocities close to stand-still (0 rpm); while full-load operation (shown as solid lines) promotes piston-pin rotational speed. The results for the full-load cases are shown as the working cycle averages for the last 3 simulated working cycles, the part-load results are shown as the total average of up to 18 working cycles due to the large variations between cycles (see text). (**b**) The average absolute angular velocity shows the magnitude of the oscillating rotational component of the piston pin, which is superimposed onto the piston-pin angular velocity.

In addition to the resulting average piston-pin rotation, the average absolute piston-pin angular velocity $\overline{|\omega_{\text{Pin}}|}$ is also investigated, which is defined as

$$\overline{|\omega_{\text{Pin}}|} = \frac{1}{b-a} \int_a^b \sqrt{\omega(t)_{\text{Pin}}^2} dt, \tag{6}$$

where a, b denote the beginning and end of the investigated working cycle.

The reason for the introduction of this additional quantity is that the piston pin does not perform a uniform rotation but has a strongly oscillating velocity component, which varies depending on operating point. This oscillating component is also able to promote hydrodynamic lubrication. As can be seen from Figure 11, the 6000 rpm full-load case shows both a very large average angular velocity as well as a very large average absolute velocity, which means that for this operating point, the piston pin does have a strong global rotation with a strong oscillation imposed. All other investigated operating points involving lower engine speeds show a much-reduced average angular velocity as well as a much slower oscillating component. It is worthwhile to note that, for example, 1000 rpm engine speed part-load conditions result in almost zero average piston-pin speed but has a strong oscillating component, while the 3000 rpm full-load case shows the exact contrary. In terms of piston-pin rotation and oscillation, the 3000 rpm part-load point yields the lowest rotation speeds. However, to assess the severity of the lubrication conditions, the piston-pin rotation and oscillation are not sufficient to give the full picture.

Therefore, the amount of metal–metal contact is investigated for the different engine operating points. The total asperity friction power loss comprises the asperity friction power losses of both piston bosses and the small end journal bearing and is shown in Figure 12 for all investigated operating points. The power loss depends on the rotation speed of the piston pin and it is interesting to note that both 3000 rpm and 6000 rpm full-load (wide-open throttle (WOT)) operating points show a similar total asperity friction power loss. However, despite this similarity, the actual rotation behaviour of the piston pin is very different as seen in Figure 11 previously: the piston pin is rotating much faster for the 6000 rpm full-load (WOT) case.
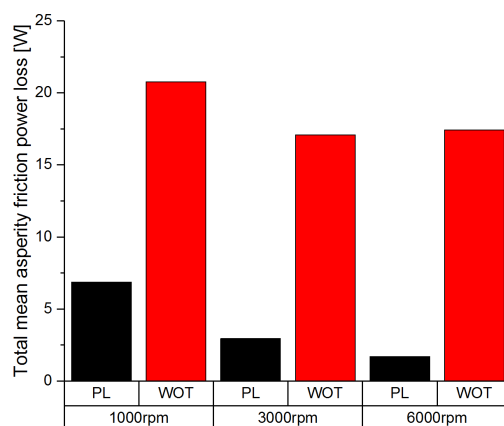

Figure 12. Plot of the total asperity friction power loss for different engine operating conditions: while full-load (WOT) operating conditions yield similar levels of mixed lubrication despite the large difference in engine speed, the total asperity friction power loss of part-load (PL) operating conditions increases with decreasing engine speed.

For part-load operation, the amount of mixed lubrication increases with decreasing engine speed, where the 1000 rpm part-load case shows the largest amount of total asperity friction power loss. This is especially severe in terms of mixed lubrication, as the rotation of the piston-pin (both net rotation speed and absolute angular velocity) is rather low, see Figure 11.

Finally, to give a more general impression of the severity of mixed lubrication, the friction power losses originating from the oil film (hydrodynamic losses) and from metal–metal contact (asperity contact losses) are shown in direct comparison in Figure 13 for two different full-load operating points. The shown

total friction power losses comprise again the friction power losses of both piston bosses and the small end journal bearings.

As can be seen, especially for the 1000 rpm full-load (WOT) operating point, the power loss due to metal–metal contact dominates strongly. For this case, the total metal–metal contact friction power loss yields a mean power loss of 20.76 W, while the hydrodynamic losses yield only an insignificant mean of 0.37 W. For the 6000 rpm full-load case, where the piston pin shows a fast oscillating and rotating movement, the asperity contact yields a mean power loss of 17.42 W and mean hydrodynamic losses of 12.46 W.
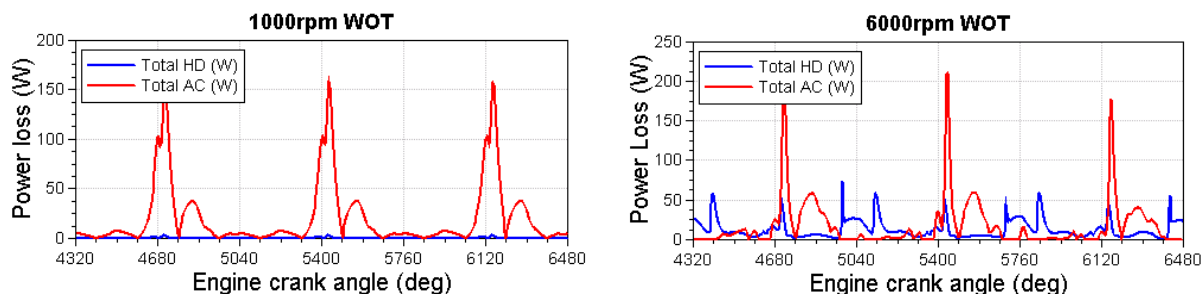

Figure 13. Total friction power loss originating from the oil film (labeled as *Total HD*) and originating from metal–metal contact (labeled as *Total AC*) for full-load operation at both 1000 rpm and 6000 rpm engine speed (3 working cycles are shown).

To summarize, the results show that engine load has a strong influence on the mixed lubrication of the piston pin; while for part-load operation, low engine speeds show increased mixed lubrication.

5. Influence of Piston-Pin Clearance

As argued earlier, the piston-pin clearance undergoes drastic changes during warm-up of the piston. It is interesting to investigate the effect of a change in piston clearance on its rotational velocity, as is shown in Figure 14.

As can be seen in this Figure 14, a change of the piston-pin clearance has a strong impact on its average angular velocity. For the piston-pin clearance of 9 μm the piston pin rotates with about −30 rpm in average. Both reduced clearances of 4 and 6 μm show a much faster average pin angular velocity of about −70 to −80 rpm. The reason for this influence can be identified in the plots of the asperity friction power losses for the piston boss and the small end (plots on the right hand side of Figure 14). With decreasing piston-pin clearance, the asperity friction power loss is increasing for the piston boss and decreasing for the small end, especially at the moment of firing.
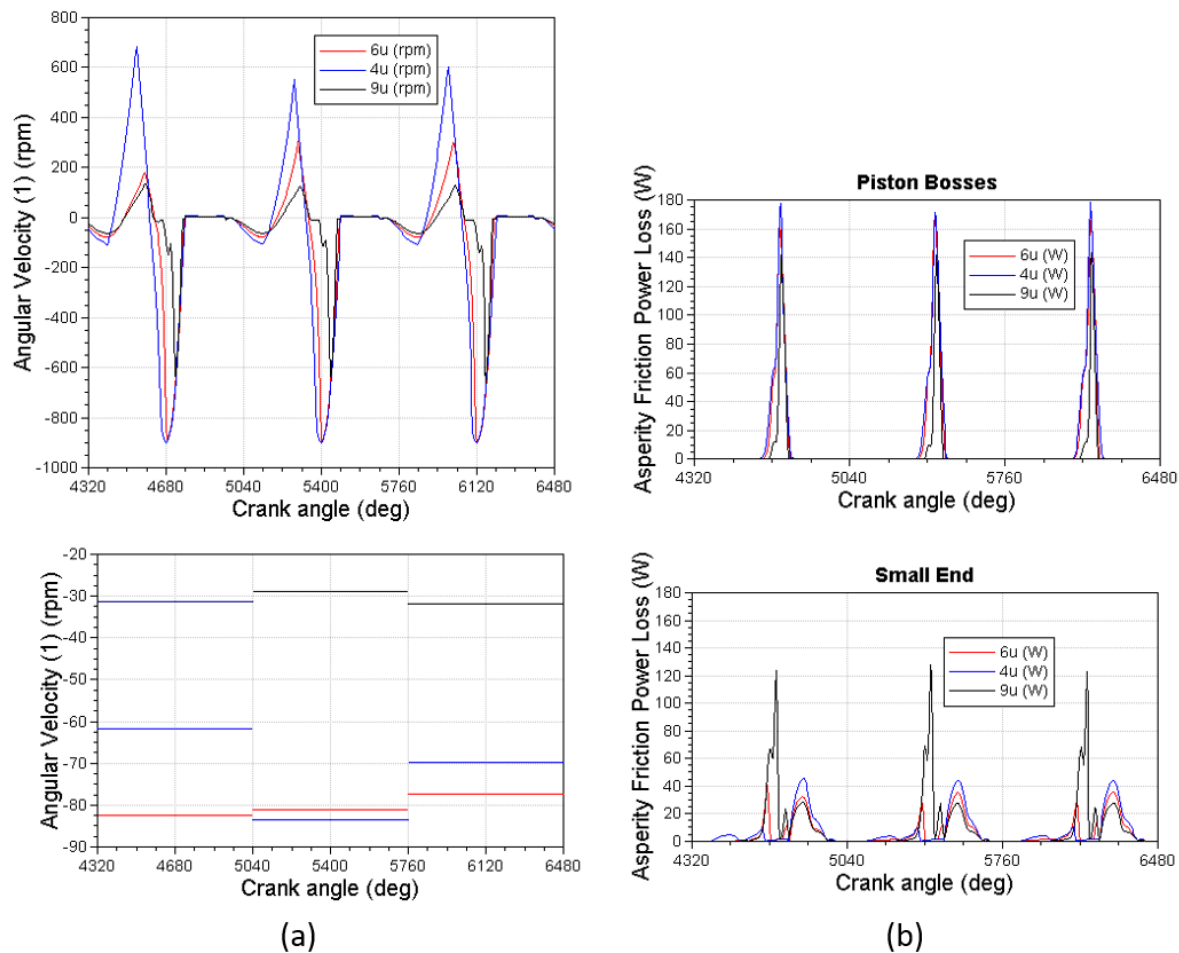
Figure 14. (**a**) Angular velocity of the piston pin for three different clearances: instantaneous angular velocity (top) and mean velocity (720° averaged) (bottom). (**b**) Plot of the asperity friction power loss of the piston bosses (top) and of the small end (bottom).

6. Influence of Piston-Pin Surface Roughness

A common strategy to reduce mixed lubrication is to reduce the surface roughness of the involved parts which generally promotes hydrodynamic lubrication. Consequently, it is investigated in the following how a significantly reduced surface roughness impacts the rotation of the piston pin and its lubrication. The reference case uses 0.06 µm surface roughness for the piston pin, the alternative case investigated for comparison employs the reduced piston-pin surface roughness of 0.02 µm.

As can be seen in Figure 15, the asperity friction power loss due to mixed lubrication reduces slightly, which is as expected. However, as the mixed lubrication in both the piston bosses and the small end is reduced at the same time, the results apparently show no net effect on the rotation of the piston pin.
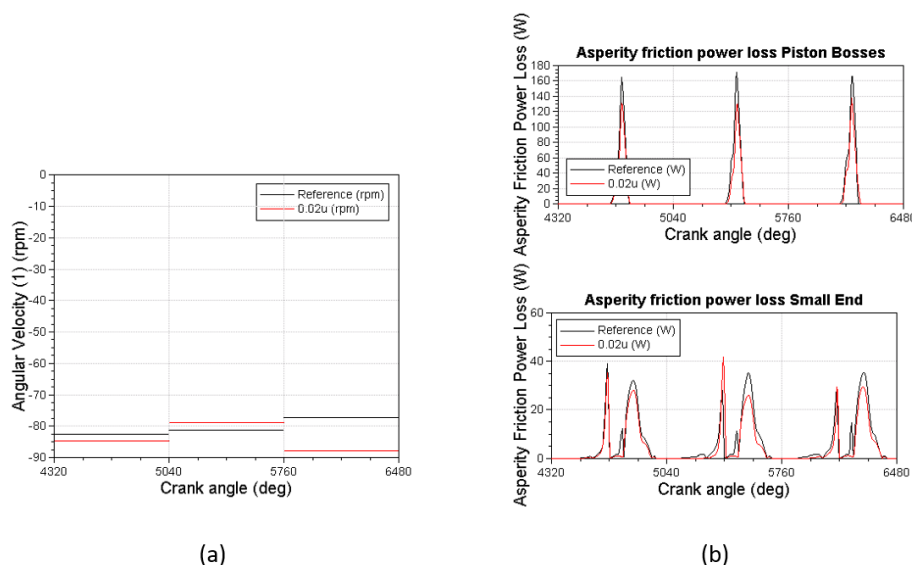
Figure 15. (**a**) Working cycle (720°) averaged angular velocities of the piston pin for two different surface roughnesses (0.06 μm for the reference and 0.02 *μm* for the alternative variant investigated) and (**b**) the asperity friction power loss of both piston bosses and small end (right); results shown for full-load/WOT operation.

7. Conclusions

To summarize, piston-pin rotation and lubrication has been investigated using an elastic EHD-simulation model involving an extensive thermomechanical simulation of the piston.

From the analysis of the influence of the engine operating conditions on piston-pin rotation, it was found that the piston-pin rotation consists of an average piston-pin rotation with a superimposed oscillating component. The exact contributions of these two motions is different for every operating condition investigated and ranges from no average piston-pin rotation with strong oscillation (as for the 1000 rpm part-load case), to significant average rotation without oscillation (3000 rpm full-load case), to even fast average rotation with strong oscillation (6000 rpm full-load case).

However, not only the range of average rotation speed and oscillation speed is diverse, the piston pin also changes its direction of rotation which indicates that there exists numerous operating conditions for which the piston pin has no average rotation speed at all.

By analyzing the asperity friction power loss to quantify mixed lubrication, it was found that the full-load operating points show the largest amount of mixed lubrication. In particular, the lowest studied engine speed of 1000 rpm showed the largest amount of mixed lubrication. Despite large differences in engine speed, this amount of asperity friction power loss is quite similar for all full-load operating points that were studied. In contrast, the part-load operating points show a much lower level of asperity friction power loss, which decreases with increasing engine speed.

The clearance of the piston pin has always been a sensitive quantity for combustion engines, as too large clearances can cause excessive knocking noise. The results from simulation confirm that smaller piston-pin clearances also promote hydrodynamic lubrication in the small end journal bearing and have a positive effect on piston-pin rotation.

Further, the influence of the surface roughness of the piston pin was investigated. The results show that the reduction of the surface roughness does have a positive effect on reducing mixed lubrication.

However, this positive effect reduces mixed lubrication in both the small end as well as in both piston boss journal bearings at the same time, so it appears that there is no net effect on piston rotation.

It is the aim of this work to provide a fundamental basis for the understanding of the lubrication of the piston pin, as well as to investigate how standard optimization measures (like changing clearance or reducing surface roughness) affect it. Future work can build on these fundamental results and extend them to actually try to predict piston-pin failure.

Author Contributions: H.A. developed the simulation model and performed the calculations; All authors analyzed and discussed the data; H.A. wrote the paper. All authors have read and agreed to the published version of the manuscript.

Conflicts of Interest: The authors declare no conflict of interest.

References

1. Open Access Publisher Intech. Available online: www.intech.com (accessed on 9 March 2020).
2. Simulia. Available online: www.simulia.com (accessed on 9 March 2020).
3. Shi, F. An analysis of floating piston pin. *SAE Int. J. Engines* **2011**, *4*, 2100–2105. [CrossRef]
4. Ligier, J.L.; Ragot, P. Piston pin: Wear and rotating motion. *SAE Trans.* **2005**, *114*, 760–768.
5. Fridman, V.; Piraner, I.; Clark, K. Modeling of mixed lubrication conditions in a heavy duty piston pin joint. In Proceedings of the ASME 2006 Internal Combustion Engine Division Spring Technical Conference, American Society of Mechanical Engineers Digital Collection, Aachen, Germany, 7–10 May 2006; pp. 741–748.
6. Suhara, T.; Ato, S.; Takiguchi, M.; Furuhama, S. *Friction and Lubrication Characteristics of Piston Pin Boss Bearings of an Automotive Engine*; Technical Report, SAE Technical Paper; SAE International: Warrendale, PA, USA, 1997.
7. Wachtmeister, G.; Hubert, A. Rotation of a piston pin in the small connecting rod eye during engine operation. *MTZ Worldw.* **2008**, *69*, 52–57. [CrossRef]
8. Iwasaki, H.; Higasa, Y.; Takiguchi, M.; Sue, S.; Shishido, K. Effects of Design for Piston Pin and Bearing on State of Bearing Lubrication. In Proceedings of the ASME 2007 Internal Combustion Engine Division Fall Technical Conference, American Society of Mechanical Engineers Digital Collection, Charleston, SC, USA, 14–17 October 2007; pp. 631–636.
9. Furuhama, S.; Tada, T.; Nakamura, T. Some Measurements of the Piston Temperatures in a Small Type Gasoline Engine. *Bull. JSME* **1964**, *7*, 422–429. [CrossRef]
10. Furuhama, S.; Oya, Y.; Sasaki, H. Temperature measurements of the connecting rod, piston pin and crankpin bearing of an automobile gasoline engine. *Bull. JSME* **1966**, *9*, 181–189. [CrossRef]
11. Furuhama, S.; Enomoto, Y. Piston temperature of automobile gasoline engine in driving on the road. *Bull. JSME* **1973**, *16*, 1385–1400. [CrossRef]
12. Furuhama, S.; Suzuki, H. Temperature distribution of piston rings and piston in high speed diesel engine. *Bull. JSME* **1979**, *22*, 1788–1795. [CrossRef]
13. Sander, D.E.; Allmaier, H.; Priebsch, H.H.; Witt, M.; Skiadas, A. Simulation of journal bearing friction in severe mixed lubrication–Validation and effect of surface smoothing due to running-in. *Tribol. Int.* **2016**, *96*, 173–183. [CrossRef]
14. Knauder, C.; Allmaier, H.; Sander, D.E.; Sams, T. Investigations of the Friction Losses of Different Engine Concepts. Part 2: Sub-assembly resolved friction loss comparison of three engines. *Lubricants* **2019**, *7*, 105. [CrossRef]

15. Knauder, C.; Allmaier, H.; Sander, D.E.; Sams, T. Investigations of the friction losses of different engine concepts. Part 3: Sub-assembly resolved friction reduction potentials and arising risks. *Lubricants* **2020**, submitted.

16. Allmaier, H.; Priestner, C.; Sander, D.E.; Reich, F. Friction in automotive engines. *Tribol. Eng.* **2013**, *8*, 149–184.

17. Sander, D.E.; Allmaier, H.; Priebsch, H.H. Friction and wear in automotive journal bearings operating in today's severe conditions. *Adv. Tribol.* **2016**, *7*, 143.

18. Offner, G. Modelling of condensed flexible bodies considering non-linear inertia effects resulting from gross motions. *Proc. Inst. Mech. Eng. Part K J. Multi-body Dyn.* **2011**, *225*, 204–219. [CrossRef]

19. Offner, G. Friction power loss simulation of internal combustion engines considering mixed lubricated radial slider, axial slider and piston to liner contacts. *Tribol. Trans.* **2013**, *56*, 503–515. [CrossRef]

20. Patir, N.; Cheng, H. An average flow model for determining effects of three-dimensional roughness on partial hydrodynamic lubrication. *J. Tribol.* **1978**, *100*, 12–17. [CrossRef]

21. Patir, N.; Cheng, H. Application of average flow model to lubrication between rough sliding surfaces. *J. Tribol.* **1979**, *101*, 220–229. [CrossRef]

22. Jakobsson, B. The finite journal bearing, considering vaporization: Report from the Institute of Machine Elements *Trans. Chalmers Univ. Technol.* **1957**, *190*, 116.

23. Sander, D.; Allmaier, H.; Priebsch, H.; Reich, F.; Witt, M.; Füllenbach, T.; Skiadas, A.; Brouwer, L.; Schwarze, H. Impact of high pressure and shear thinning on journal bearing friction. *Tribol. Int.* **2015**, *81*, 29–37. [CrossRef]

24. Allmaier, H.; Priestner, C.; Reich, F.; Priebsch, H.; Forstner, C.; Novotny-Farkas, F. Predicting friction reliably and accurately in journal bearings–The importance of extensive oil-models. *Tribol. Int.* **2012**, *48*, 93–101. [CrossRef]

25. Morina, A.; Neville, A. Understanding the composition and low friction tribofilm formation/removal in boundary lubrication. *Tribol. Int.* **2007**, *40*, 1696–1704. [CrossRef]

26. Greenwood, J.; Tripp, J. The contact of two nominally flat rough surfaces. *Proc. Inst. Mech. Eng.* **1970**, *185*, 625–633. [CrossRef]

27. Priestner, C.; Allmaier, H.; Priebsch, H.; Forstner, C. Refined Simulation of Friction Power Loss in Crank Shaft Slider Bearings Considering Wear in the Mixed Lubrication Regime. *Tribol. Int.* **2012**, *46*, 200–207. doi:10.1016/j.triboint.2011.03.012. [CrossRef]

28. Allmaier, H.; Priestner, C.; Reich, F.; Priebsch, H.; Novotny-Farkas, F. Predicting friction reliably and accurately in journal bearings - extending the simulation model to TEHD. *Tribol. Int.* **2013**, *58*, 20–28. [CrossRef]

29. Etsion, I.; Halperin, G.; Becker, E. The effect of various surface treatments on piston pin scuffing resistance. *Wear* **2006**, *261*, 785–791. [CrossRef]

30. Haque, T.; Morina, A.; Neville, A.; Kapadia, R.; Arrowsmith, S. Effect of oil additives on the durability of hydrogenated DLC coating under boundary lubrication conditions. *Wear* **2009**, *266*, 147–157. [CrossRef]

31. Knauder, C.; Allmaier, H.; Sander, D.E.; Sams, T. Investigations of the Friction Losses of Different Engine Concepts. Part 1: A Combined Approach for Applying Subassembly-Resolved Friction Loss Analysis on a Modern Passenger-Car Diesel Engine. *Lubricants* **2019**, *7*, 39. [CrossRef]

32. Zhang, J.; Piao, Z.; Deng, L.; Zhang, S.; Liu, J. Influence of pin assembly on the wear behavior of piston skirt. *Eng. Fail. Anal.* **2018**, *89*, 28–36. [CrossRef]

33. Moshrefi, N.; Mazzella, G.; Yeager, D.; Homco, S. *Gasoline Engine Piston Pin Tick Noise*; Technical Report, SAE Technical Paper; SAE International: Warrendale, PA, USA, 2007.

34. Kondo, T.; Ohbayashi, H. *Study of Piston Pin Noise of Semi-Floating System*; Technical Report, SAE Technical Paper; SAE International: Warrendale, PA, USA, 2012.

35. Enomoto, Y.; Furuhama, S.; Minakami, K. Heat loss to combustion chamber wall of 4-Stroke gasoline engine: 1st report, heat loss to piston and cylinder. *Bull. JSME* **1985**, *28*, 647–655. [CrossRef]

36. Morel, T.; Keribar, R.; Harman, S. Detailed analysis of heat flow pattern in a piston. In Proceedings of the International Symposium COMODIA, Kyoto, Japan, 3–5 September 1990; Volume 90, pp. 309–314.